24th EUROPEAN ROTORCRAFT FORUM
Marseilles, France - 15th-17th September 1998

FM 04

Examination of the heave axis aeromechanics of a hovering helicopter

A T McCallum
P C Tarttelin
C P Sugrue
Flight Management and Control Department
Defence Evaluation and Research Agency
Bedford
United Kingdom

Presented in this paper are the results from a study of the physical effects which underlie the heave axis response of a hovering helicopter. Experimental data gathered during a series of flight tests using the DERA aeromechanics Lynx are used to reconstruct a comprehensive picture of rotor behaviour, including deflection of the main rotor blades and distribution of aerodynamic loading across the main rotor disc. Data gathered from a heave axis control input are then compared with equivalent data derived from a high order model of the Lynx. In particular, two configurations of the Peters-He generalised finite-state inflow model are compared. It is shown that both models are able to characterise the heave-axis response with a high degree of fidelity, although some deficiencies in the off-axis responses remain. While the change in inflow structure is found to have little impact upon the overall vehicle response, the higher order inflow model captures more faithfully the radial distributions of both incidence and inflow.

1. INTRODUCTION

1.1 Role of high-fidelity flight dynamics modelling

Simulation plays an important role at almost every stage in the life of a military rotorcraft, from air fleet sizing through to mid-life updates and disposal. Traditionally, simulation modelling is used for performance estimation, loads analysis and flying qualities. In many cases, the flying qualities models are of relatively low fidelity in relation to the others, due to the need for real-time execution.

However, the availability of high-fidelity flying qualities models during the design stage is crucial to the early identification of handling qualities cliff-edges and other objectionable behaviour which could restrict the aircraft in its operational role. Too often, these handling limitations are discovered, not through piloted simulation, but during the flight testing of prototype airframes, by which stage considerable investment of time and effort has been expended. Opportunities are available, using modern control techniques, to operate the military helicopter close to the edge of its operational flight envelope (OFE). This requires a very high level of confidence in the simulation model's predictive capability, as it is in these flight regimes where handling problems arise. Ironically, it is in these regimes where the physics of the vehicle is least well understood.

1.2 High-fidelity rotor modelling

Helicopter rotor modelling can be regarded as the interaction of three components; the aerofoil aerodynamics, the induced flow theory and the rotor dynamics, as illustrated in Figure 1 (adapted from [1]). As depicted, the aerodynamic incidence is a combination of three components; the blade pitch applied through the flight control system, the inci-

dence due to the motion of the blade relative to the surrounding air and, finally, the incidence due to the induced flow through the rotor. As indicated by the feedback loops, the latter contributions are indirectly influenced by the blade incidence.

Simulating the physical processes which occur within each of the blocks in the diagram and ensuring that the complexity and fidelity available in one block is consistent with that contained in the others, is possibly the single-most significant challenge facing flight dynamics and rotor dynamics engineers. This challenge is most acute in the realm of real-time, piloted simulations, where, despite continually improving computer performance, the model complexity needs to be traded off against real-time execution capability.

1.3 DERA's high-fidelity simulation research programme, HiFiSim

For a number of years, DERA has been funded, through the UK Ministry of Defence's Corporate Research Programme, to conduct research into the requirements for high fidelity simulation models applied to flight control, handling qualities and piloted simulation studies. The study, known as HiFiSim, has consisted of two major activities

a) flight testing for validation data

b) assessment of model structures and validation techniques.

In this paper, the results are presented from a study in which these two activities were drawn together and focused upon the heave axis response of a hovering Lynx helicopter.

1.4 Structure of paper

In Section 2 a brief review of the DERA experimental aeromechanics Lynx aircraft and its instrumentation suite is presented. Following this, in Section 3, is a description of the analysis techniques used to reconstruct a comprehensive picture of rotor behaviour, including deflexion of the main rotor blades and distribution of aerodynamic loading across the main rotor disc.

Section 4 contains a summary of the simulation model employed in this study together with details of the inflow models examined. In Section 5 a heave axis manoeuvre is described, followed in Section 6 by comparisons of flight test and simulation. Finally, in Sections 7 and 8 the main findings of the study are reviewed.

2. THE DERA AEROMECHANICS RESEARCH LYNX

2.1 Lynx ZD559

The flight test data presented in this paper were gathered using DERA Lynx ZD559 (known as ALYCAT - the Aeromechanics Lynx Controls and Agility Testbed), operated from DERA Boscombe Down. Following its arrival at DERA in 1985, the aircraft was instrumented with control position potentiometers, cabin accelerometers, rate and attitude gyros, and a Modular Data Acquisition System (MODAS) for recording these sensors together with speed and altitude sensors in the standard aircraft air data unit.

Further improvements made to the instrumentation included the addition of engine sensors, the Helicopter Air Data System (HADS) for the measurement of true air speeds in all three axes, tail rotor strain and pressure instrumentation. A suite of Fatigue and Usage Monitoring (FUM) sensors composed of strain gauges on the main rotor head (MRH), main rotor blades and gear box, tail boom and tail rotor shaft were also installed.

To support rotor aeromechanics research a major installation of MRH instrumentation was performed. This is composed of an instrumented MRH and blades, a MRH electronics platform for sensor output amplification and multiplexing, a slip ring assembly for transfer of the rotating system data to the non-rotating instrumentation, and Virtual Memory Equipment (VME) acquisition and demultiplexing units for data transfer to the MODAS. The MRH instrumentation consists of strain gauged elements used for measuring responses to hub element flexure, shaft torque, rotor pitching motion and control rod loads.

2.2 The LYNXRIBs

Most pertinent to this paper are the two Lynx instrumented rotor blades known as the LYNXRIBs [2] and composed of the Pressure Instrumented Blade (PIB) and the Strain Gauged Blade (SGB). Figure 2 shows the location of sensors on these blades.

SGB: the 42 strain gauge bridges on this blade and its MRH arm are used to obtain blade flap, lag

and twist displacement data through the use of a modal fitting procedure known as Strain Pattern Analysis (SPA) [3].

PIB: the 81 pressure sensors located on the PIB are used for the calculation of blade incidence and loading using the indicator method [4] and consist of:

a) 20 radially distributed leading edge sensors, for calculation of local force and incidence;

b) 20 radially distributed trailing edge sensors, used as flow separation indicators;

c) 22 chordwise sensors at 85% radius (shown in Figure 3), for validation of the indicator method in 2-D flow (discussed later in this section);

d) 22 chordwise sensors at 98% radius, for evaluation of the indicator method in 3-D flow;

e) 1 tip pitot sensor at 99% radius.

Together these blades are able to provide the blade load and displacement data necessary for detailed model validation.

3. FLIGHT DATA PROCESSING AND RECONSTRUCTION

3.1 Data recording and storage

Data recorded to the MODAS system are replayed, post-flight, onto a PC-based data server. This system was purpose built for the DERA HiFiSim programme to enable more rapid access to a large variety of test points, allow searching for comparable test points and permit access to every available recorded data sample from rotor start-up and take-off through to landing.

Analysis of the main rotor data is centred around the RIBAN (Research Instrumented Blade Analysis) software package [5]. Originally written for the GPRIB (General Purpose Research Instrumented Blade) flown on the RAE research Puma, this package uses the rotor measurements to calculate blade displacements, incidence and loading [6] over a range of azimuthal and radial stations.

3.2 Reconstruction of blade structural dynamics

Blade flap, lag and twist displacements are reconstructed from the raw strains using the Strain Pattern Analysis (SPA) technique [3]. These are synthesised (Figure 5) through reference of blade in-flight strains with those obtained from a non-rotating modal calibration [7] using a weighted least squares error technique [8].

3.3 Reconstruction of blade aerodynamics

Local blade incidence, normal force coefficient and pitching moment coefficient are estimated from raw pressures using the Incidence Indicator Method (IIM) [4] (see Figure 4). This method was developed to resolve forces on the blade from a single pressure sensor placed near to the leading edge (2% chord). The method is reliable provided that there is no flow separation (i.e. stall) and the flow can be considered two-dimensional i.e. away from the tip region of the blade, and interpreted with caution during close blade tip vortex interaction.

The IIM makes use of look-up tables constructed from wind tunnel data, and which are referenced by the local Mach number (M) and leading edge pressure coefficient (C_{pLE}). These two parameters, through the look-up tables, return normal force coefficient (C_N), aerodynamic incidence (α) and pitching moment coefficient (C_m) [9].

Confidence in the IIM has been obtained from analysis of the chordline array of sensors mounted on the PIB at 85% radius [10]. Comparison of the lift obtained by integration of the chordwise pressures with that predicted from the two-dimensional look-up tables at similar conditions demonstrated good agreement, and by inference a corresponding agreement of incidence values.

Having constructed a comprehensive picture of the rotor structural dynamics and aerodynamics, RIBAN is able to decompose the measured incidence into estimates of the contributions from applied blade pitch, blade deflection and induced flow (i.e. the summing junction components in Figure 1). This provides a comprehensive picture of the rotor aeromechanics and is suitable for use in rotor model validation studies.

Finally, since the PIB is a non-standard blade, RIBAN calculates an additional data set, that adjusts the PIB data to represent a standard metal blade. The basis of the adjustment is to 'remove' the PIB tip

fairing and adjust the overall blade pitch and incidence such that the resulting root flap bending moment remains unchanged, thus effectively maintaining the moments that describe the tip path.

3.4 Data quality analysis

Data quality analysis can be performed at a number of levels within the system. The lowest level addresses problems at the individual channel level, in particular the removal of data drop outs. The impact of leaving drop-outs in the data varies depending upon the channel affected. For example, if the channel is a single strain gauge on the SGB, then the drop out will affect the entire displacement distribution for all 3 axes (flap, lag and torsion) due to the synthesis used in the Strain Pattern Analysis (SPA) process. If the channel is a pressure sensor, then a peak or drop in the rotor lift distribution at a single point will be seen. Algorithms for automatic removal of drop-outs are being developed.

At a higher level, the overall data quality is assessed using reconstructed data. For example, calculation of the integrated rotor thrust from the PIB can be compared with the known aircraft weight, and reconstructed inflow velocities can be compared with theoretical inflow velocity (e.g. momentum theory).

The most significant data quality issue encountered during the current study was concerned with measurements of main rotor blade feather angles. These were measured using a cam and follower arrangement mounted at the blade pitch bearing. Extensive static calibrations relating pilot controls to blade feather angles and control servo positions were conducted. However, it was found that during flight the correlation between the measured feather gauge angles and those which would be expected from the equivalent servo positions was significantly degraded. In addition, significant variations were found between measured blade root angles. These were attributed to two primary factors :-

a) The root feather angle measurements contain the control system input, the control system flexures and the main rotor blade pitch-flap coupling (δ_3) effects. Not all of these can be captured in a static calibration.

b) The four blades have differing distributions of mass and aerodynamic characteristics, and hence give different δ_3 responses.

Work is currently being done to account for the δ_3 component using modal methods from SPA to correct the pitch results and also to account for the control system flexibility for the servo-predicted results.

However, in the data presented herein, the δ_3 component had not been fully accounted for and as a result, the RIBAN software, which is reliant upon accurate knowledge of feather angles, produces errors in the reconstructed inflow angle. Thus, the results given in this paper focus on *qualitative* comparisons of inflow distribution.

4. DESCRIPTION OF THE SIMULATION MODEL

4.1 Lynx air vehicle model

In this study all simulations were performed using FLIGHTLAB [11], a comprehensive simulation development and analysis system. For this study, the main rotor model consisted of a modal representation of main rotor elasticity, using lookup tables to calculate blade section aerodynamic coefficients, indexed by incidence and mach number. The tail rotor was approximated as a quasi-steady actuator disc while the fuselage and empennage aerodynamics were obtained via table look-up of wind-tunnel derived data. The main rotor inflow was modelled using two configurations of the Peters-He inflow model, details of which are given later in this section.

It is noted that while the test aircraft was a Lynx Mk 7 the model had been configured using Lynx Mk 5 data. The differences between these variants relate to the tail rotor parameters including direction of rotation. Prior experience of these changes in other simulations indicated that no major influence on the overall aircraft response to main rotor control inputs would be expected. As discussed earlier, the main rotor blades on the test aircraft were modified to accommodate the pressure and strain instrumentation, making them dissimilar. These modifications were not modelled for this study, but the correction of the flight test data to standard blade conditions enables a reasonable *qualitative* comparison of flight and simulation to be made.

4.2 Main rotor inflow model

Modelling of rotor inflow, the flow induced in the air surrounding the rotor in reaction to its thrust and hub moments, has seen a number of important advances over the past twenty years [1]. Rotor thrust is non-uniform, exhibiting both spatial and temporal

variations according to the state of the aircraft and the loading of the rotor. Modelling this flow field for flight dynamics application is challenging in two main respects:

a) The flow field is a continuum described by a set of partial differential equations. No general closed form solutions to these equations exist and numerical solution methods are currently inappropriate for real-time applications.

b) The transformation of the flow field from a continuum, of infinite dimension, to a finite set of ordinary differential equations must address the spatial and temporal nature of the flow.

Early attempts at modelling the inflow assumed that the flow reacted instantaneously to changes in thrust. While this was recognised as a deficiency, their application was generally limited to estimation of steady rotor loads and helicopter performance calculations, where the dynamic nature of the flow was of limited interest. Where dynamic effects were of interest, these could be approximated through use of lift deficiency factors and other corrections which influenced the rotor damping. However, as the use of simulation to support flight control system development and piloted simulation became more widespread, the need to capture the dynamic nature of the flow became more important.

One major advance was the development by Pitt and Peters [12], of an inflow model which satisfied the fluid flow continuum equations approximately but which was sufficiently simple that it could be incorporated readily in real-time simulations. Expressing the time-wise variation of the inflow components in first order, matrix-vector form, this model calculated the inflow at any point of the rotor disc from a combination of uniformly and harmonically distributed components, i.e.

$$\lambda(\bar{r},\psi,t) = \lambda_0(t) + \bar{r}(\lambda_s(t)\sin\psi + \lambda_c(t)\cos\psi) \qquad (4\text{-}1)$$

where $\bar{r}$ and ψ are the (normalised) radial and azimuthal position of the calculation point, λ_0 is the uniform component of inflow and λ_s, λ_c are the sine and cosine harmonic components.

This structure was ideally suited to simulations where the rotor blades were assumed to be rigid, as the mode shapes of the blades were well matched to those of the inflow distribution. However, its use in rotor models which include higher order elastic modes is questionable, an example of the need for the blocks in Figure 1 to be of commensurate complexity.

4.3 The Peters-He finite state inflow model

In a continuation of Pitt and Peters' work, Peters and He [13] returned to a more general representation, where the inflow at a point on the disc was defined to be the summation of an arbitrarily large but finite number of modal contributions, i.e.

$$\lambda(\bar{r},\psi,t) = \sum_{m=0}^{N}\sum_{j=m+1,m+3,\ldots}^{S}\phi_j^m(\bar{r})\left[\alpha_j^m(t)\cos(m\psi) + \beta_j^m(t)\sin(m\psi)\right] \qquad (4\text{-}2)$$

where $\bar{r}$ and ψ are the normalised radial and azimuthal positions of the point, N is the number of retained azimuthal harmonics, S is the number of mode shapes and ϕ_j^m is the mode shape relating the m^{th} harmonic to the j^{th} mode shape.

Analogous to the lambdas of the Pitt-Peters model, α_j^m, β_j^m are the time varying modal weights of the mode ϕ_j^m. These modes are constructed from Legendre polynomials which can be shown to satisfy Laplace's equation across the plane of the rotor disc. The response of the modal weights to changes in rotor loading is governed by a set of ordinary differential equations of the form,

$$M\dot{\underline{x}} + L\underline{x} = \underline{Q} \qquad (4\text{-}3)$$

where $\underline{x} = \left[\underline{\alpha}^T \quad \underline{\beta}^T\right]^T$ is the state vector of modal weights, M and L are, respectively the modal mass and static gains matrices, while $\underline{Q}$ is the vector of aerodynamic loads generated by the rotor.

The ability to select an arbitrarily large number of modes is an extremely attractive property of the Peters-He model and allows its use in a wide range of rotor simulation applications; from rotor performance analyses, using many modes, to flight dynamics applications using substantially fewer modes. In this study, the objective was to start from a baseline configuration of the inflow model and assess the need for additional modes when simulating the heave-axis response to control inputs.

4.4 Models used in the current study

For the study discussed here, comparisons were made between two different configurations of the Peters-He model. The first of these was a three state model consisting of a single zeroth harmonic mode and a single first harmonic mode, resulting in the following inflow calculation

$$\lambda(\bar{r},\psi,t) = \alpha_1^0(t)\phi_1^0 + \phi_2^1(\bar{r})\left(\alpha_2^1(t)\cos(\psi) + \beta_2^1(t)\sin(\psi)\right) \quad (4\text{-}4)$$

for which $\underline{x} = \left[\alpha_1^0\ \alpha_2^1\ \beta_2^1\right]^T$. This was selected for its similarity to the Pitt-Peters model structure.

The second configuration consisted of six states representing the contribution of two zeroth harmonic modes, a single first harmonic mode and a single second harmonic mode. In this case the inflow was calculated from

$$\lambda(\bar{r},\psi,t) = \alpha_1^0(t)\phi_1^0 + \alpha_3^0(t)\phi_3^0 + \phi_2^1(\bar{r})\left(\alpha_2^1(t)\cos(\psi) + \beta_2^1(t)\sin(\psi)\right) + \phi_3^2(\bar{r})\left(\alpha_3^2(t)\cos(2\psi) + \beta_3^2(t)\sin(2\psi)\right) \quad (4\text{-}5)$$

for which $\underline{x} = \left[\alpha_1^0\ \alpha_3^0\ \alpha_2^1\ \alpha_3^2\ \beta_2^1\ \beta_3^2\right]^T$.

It should be noted that each *harmonic* mode is associated with two states and that the modes used in the three state model constitute a subset of those used for the six state model.

The full set of modes is illustrated in Figure 6. Perhaps of most immediate interest is the second of the two zeroth harmonic modes, ϕ_3^0, which has a domed appearance. This is of interest to the current study as it has the potential to influence significantly the spanwise distribution of inflow. Also of interest is the second harmonic mode which has a saddle-like appearance, illustrating the coupling of radial and azimuthal flow variations. This selection of modes represents the first step forward from the three state Pitt-Peters model and is only one of the many which may be used for flight dynamics studies.

5. ANALYSIS OF LYNX HEAVE AXIS MANOEUVRE

5.1 Description of the flight test manoeuvre

The test case examined here is a heave axis input, similar to that which would be conducted operationally during low-level, nap-of-the-earth flight. As shown in Figure 7, the manoeuvre is initiated with a 5% change in collective, followed by a modest pedal input to limit excursions in the yaw axis. Despite this, a steady yaw rate of 10 deg s^{-1} develops producing around 70 deg of heading change over the duration of the manoeuvre. The aircraft response is allowed to develop for approximately eight seconds, during which time the roll rate increases to around 8 deg s^{-1} and the roll attitude to around 20 deg, whereupon the pilot recovers control of the aircraft.

Also shown in the figure is an estimate of the height rate response, calculated from the measured normal acceleration. Using a simple first order model of the acceleration response, allows the heave axis damping and control power derivatives to be estimated. These are presented in Figure 8 where it can be seen that although the longer term response is well predicted, the higher order dynamics present during the transient portion of the acceleration response, cannot be reproduced by the first order approximation. The associated estimate of height rate is relatively good, showing the correct trend throughout the manoeuvre, although offset by around 0.2 m s^{-1}. This is in general agreement with previous DERA studies using Puma flight test data [14].

The least squares analysis identifies Z_w = -0.202, which is around 60% of that expected from momentum theory, and this anomaly is felt to be due to the presence of noise during the transient response. A more reliable estimate can be obtained by analysing the height rate response directly using the algorithm defined in ADS 33 [15]. This indicates a borderline Level 1/2 response with τ = 0.198s and T = 3.672s.

5.2 Examination of the rotor aeromechanics

In Figure 10 the blade incidence data derived from the leading and trailing edge pressures on the PIB are presented for selected revs during the manoeuvre. These revs represent data for steady hover (rev 9), the collective control input (18, 19), post-input response (20, 25) and immediately before pilot recovery (58). In all cases the data are presented as

polar plots where the shading represents the incidence levels (after correction to standard blade conditions). It is emphasised that the data are continuous time histories, throughout one revolution (anticlockwise when viewed from above) Hence discontinuities are present between the beginning and end of each rev where the aircraft motion is unsteady. Zero degrees azimuth is to the rear of the aircraft.

The collective input begins at the start of rev 18 where it can be seen that there is a slight reduction in inboard incidence relative to rev 9; elsewhere there is a small increase, but in general the distribution shape remains the same. The input ends at the end of rev 19; again, the distribution remains very similar, although the incidence has in general risen by about 0.75°. Rev 20 is the first full rev post-input; the tip activity near the end of the rev has diminished slightly but otherwise it shows the features of the steady hover. Approximately one second later, rev 25 again reveals little change except in the tip region near the end of the rev, but after a further 6 seconds the distribution has changed; rev 58 displays an absence of the tip effects, except where an upwash (increase in incidence) is expected at the front of the disc as a result of the aircraft accelerating from 8.5 to 9.5 knots at a sideslip increasing from 6° to 8°. This is accompanied by a corresponding downwash (reduction of incidence) over the rear of the disc and upwash at the blade root visible between 150° and 180° azimuth. The majority of the distribution remains fairly flat, however, with a maximum variation of about 2°.

5.3 Consistency of aerodynamic loads with measured acceleration

The azimuthal and radial loading from the PIB can be integrated to provide the time averaged thrust and moments for each main rotor revolution. The average thrust over rev 1 from F368 E19 (assuming all four blades to be loaded as per the PIB) is 9% higher than the estimated aircraft weight (at 1 g) which can be accounted for in part by the download experienced between the main rotor and fuselage.

The 'standardised' calculation (described in 3.1) reduces this over prediction to about 6%. In Figure 9, the calculated thrust is normalised to that of rev 1 to remove this general over prediction for clearer comparison with the rev-by-rev averaged normal acceleration (in g). It can be seen that the initial accelerometer output indicates a slight (and increasing) downward acceleration during the steady hover phase which is matched by the calculated thrust. The slope of both measurement and calculation during the input is matched, and although the measured acceleration overshoots and oscillates at the end of the input, the general trend of both sets of data is very similar up to the point of recovery. The differences could be due to changes in the rotor-fuselage download throughout the input and the dynamic characteristics of the accelerometer. In general though, these results provide an important validation of the aerodynamic measurements despite the presence of three-dimensional flow and unsteady aerodynamics.

6. COMPARISON OF MEASURED AND SIMULATED FLIGHT DYNAMICS

6.1 Simulation of the vehicle response

Figure 11 illustrates the measured and simulated responses of the fuselage normal acceleration, rates and attitudes. It is noted that, for clarity, only the 3-state simulation results are shown. Generally, the 3- and 6-state simulation results were very similar across most of the manoeuvre and the following comments apply equally to each.

Of most interest are the comparisons of the normal acceleration and velocity, the primary on-axis responses for collective inputs. As shown in the figure, the acceleration response is generally well predicted. Peaking at about 1.15 m s^{-2} within half a second of the input being applied, the simulation under predicts the flight test by around 20% (compared with 40% for the linear theory in Figure 8). The longer term comparison is good, with the simulation and flight overlaying up to the recovery point. The most obvious anomaly occurs during the first three seconds of response, where the measured data exhibits a higher order dynamic response than the simulation. However, it should be recalled that the test aircraft used in the present study was equipped with dissimilar rotor blades, which despite being tuned for steady flight conditions, are likely to have dissimilar transient responses. Another possibility is that the disturbed acceleration response may be due to an external disturbance such as a gust.

Associated with the normal acceleration is the height rate response which is also seen to be well predicted, although offset by around 0.2 m s^{-1} across most of the event. However, this offset arises mainly from the fact that the height rate response is non-zero at the point when the input is applied. Unlike the

simple linear theory of Figure 8, the FLIGHTLAB model appears to capture more faithfully the peak acceleration. It also gives good predictions of both control power and heave damping. Thus for piloted simulation applications, the model would appear to handle much the same way as the real aircraft, offering a higher fidelity representation of the Lynx than would be possible using quasi-steady theory.

Turning now from the on-axis response to off-axis, coupled responses, it is apparent that the cross-coupling from collective to yaw is, in the short term, reasonably well predicted (see lower part of Figure 11). The simulation response is slightly advanced of the flight response, which appears to exhibit a non-minimum phase characteristic. Long term, the measured and simulated responses depart, with the measured response obtaining a relatively steady value of 10 deg s^{-1} while the simulated response washes off and, eventually, reverses direction. These discrepancies can be attributed, to the modelling of the relationship between the pilot's pedals and the tail rotor collective. Reducing the gain between pedal and blade angle prevents the wash-off and reversal, although the justification for so doing requires further investigation. Furthermore, the aerodynamic loads produced by the fuselage and tailboom would provide additional yaw damping. The influence these modification have on simulation of the Lynx in low speed flight has recently been reported [16] but were unavailable at the time the FLIGHTLAB model was constructed.

The other coupled responses are relatively poorly predicted. While the pitch rate response is of the right magnitude, it is of the opposite sign to the flight test data. Like the yaw axis response, this may be due to a deficiency in the modelling of the interlink between the collective and longitudinal cyclic channels or in the accurate placement of the fore/aft centre of gravity within the simulation, and these certainly warrant further investigation. The simulated roll rate and attitude are similarly in error, with the latter being approximately half that of the flight test and in the opposite direction. In addition, the simulated roll rate contains a low-frequency oscillation not present in the flight test. It is well known that the main rotor regressing lead-lag mode can become coupled with the roll axis and it is suggested that it is this mode which is apparent in the simulated data. It is difficult to see from a visual inspection of the flight test data whether such a mode is present within the flight test data and thus no conclusions can be drawn at this point about the fidelity of the simulation in this area.

While the comparison of the vehicle's rate and attitude response has raised a number of items for further investigation, it is noted that changing the structure of the inflow model made little change to the simulation of the short term flight dynamics response and had negligible impact upon the primary heave axis response. The question remains as to whether the detailed modelling of the structural and aerodynamic response of the rotor is substantially influenced by changes to the modal content of the inflow model.

6.2 Simulation of the rotor response

A useful starting point for assessing the simulation of rotor response is the average blade flapping displacement, or coning. Flight test coning has been derived from the reconstructed blade deflection data (see 3.2) and a rev-by-rev average constructed for a number of rotor revolutions during the manoeuvre. This is shown in Figure 12 along with the coning response from the three and six state inflow models. The discrepancy between flight and theory should be similar to the comparisons of normal acceleration if the mass and radial distributions are constant. This appears to be the case, with both models underpredicting the coning by up to 20% in the short term, but providing reasonably good predictions in the longer term.

Sources of discrepancy between simulation and flight include, as before, the dissimilarity of the rotor blades on the test vehicle, the possibility of an external disturbance such as a gust, and differences between the modal content of the blade response in flight and those incorporated in the simulation model. As before, these warrant further investigation, however, of immediate interest is the difference between the two simulation models. In particular, the three state model attains a peak value of coning which is around 0.04 degrees larger than that for the six state model and this offset is sustained throughout the manoeuvre. No such differences between the models were observed for the predictions of normal acceleration, suggesting that while the overall rotor thrust has been unaffected by alteration of the inflow model, the distribution of thrust across the disc has been altered. Specifically, the slightly larger peak in coning seen for the three state model indicates a greater concentration of thrust at the blade tips, in turn suggesting a higher aerodynamic incidence in

the tip region. Similar behaviour in the flight test data may also indicate an even greater increase of incidence near the blade tip.

The blade incidence distribution, reconstructed from the flight test measurements of leading and trailing edge pressures (see 3.3), is shown in Figure 13 together with equivalent data produced by the two simulation model configurations. It should be noted that all of these data have been averaged on a rev-by-rev basis and so what is being presented is the variation in the zeroth harmonic components of inflow.

Examination of the flight test data reveals the presence of a tip-vortex interaction [4], giving rise to the sharp increase in incidence over the outer 20% of the blade. Following the input and during the initial peak acceleration phase of the manoeuvre, the spanwise peak incidence occurs very close to the blade tip and throughout the remainder of the manoeuvre migrates inboard to 85% span at the point of recovery. It is immediately apparent that neither of the simulation models has captured this behaviour, a matter which is unsurprising given that the radial variation of the inflow modes was limited to second order.

It is equally apparent that the incidence distributions present in the two simulations are quite different, with the three state model predicting a general *increase* from root to tip, while the six state model predicts a general *decrease* from root to tip, indicating a higher inboard loading. This can be attributed to the presence in the six state model of the zeroth harmonic mode ϕ_3^0 which has a domed appearance (Figure 6).

A further comparison of the simulations with flight test is given in Figure 14 where spanwise variation of incidence is shown for a number of the rotor revs discussed in 5.2. Once more, the presence of the tip-vortex interaction is clear in the flight test data as is the fact that neither simulation model is able to capture its characteristics. As inferred from the simulated coning responses, the incidence predicted by the three state model is generally higher near the blade tip than that of the six state model and remains so throughout the manoeuvre. Over the inboard portion of the blade, between 45% and 60% of the blade span, the three-state model under-predicts the flight test incidence by around 0.5 deg. In contrast, the six state model provides a good prediction of incidence for the portion of the blade between 40% and 70% throughout the initial phase of the manoeuvre. The deterioration beyond 75% of blade span point is probably due to the influence of the tip-vortex and its migration inboard.

Finally, Figure 15 shows the comparison of mean induced flow averaged over one revolution reconstructed from flight, with that predicted by the simulations. While it is noted that both models under-predict the mean inflow significantly it is recalled that the accuracy of the inflow reconstruction is questionable, due to its sensitivity to changes in blade feather angle which, as discussed in 3.4, proved difficult to calibrate with a high degree of certainty. It is important to note however, that the six state model has accurately reproduced the spanwise variation in the non-harmonic inflow component and that this would simply not be possible within the confines of a three state simulation model.

7. DISCUSSION

The foregoing observations serve to illustrate the influence which a fairly modest alteration of the rotor inflow model can have upon the prediction of fundamental rotor parameters such as flapping, incidence and inflow. When examined in conjunction with the overall prediction of flight dynamics responses to controls, it would appear that implementation of a higher order inflow model would be unjustified for handling and control activities. In particular, the addition of a second harmonic inflow component has no useful effect upon inter-axis coupling. However, these arguments can be tempered when it is recalled that the application of piloted simulation models continues to extend beyond that of six degree-of-freedom stability and control analysis. Indeed, as primary flight control extends into rotor state feedback and smart rotor technology, the accurate prediction of localised aerodynamic effects will gain increased importance. These early results suggest model structures which satisfy the objectives of both flight dynamic and rotor dynamic simulations are possible using current generation modelling theory.

8. CONCLUSIONS

In this paper the results from a study of the aeromechanics of a hovering helicopter have been presented. The ALYCAT Lynx experimental aircraft facility, operated by the UK's Defence Evaluation and Research Agency (DERA), has been reviewed and details of its instrumentation and post-flight data analysis capability discussed.

Data from this facility have been compared with equivalent data simulated by a high order flight dynamics model and in particular, two configurations of the Peters-He finite state wake model. Despite the fact that uncertainty in the blade feather angles limits the ability to draw definitive *quantitative* conclusions, the following *qualitative* conclusions can be drawn.

With regard to the prediction of *vehicle* aeromechanics :

a) Heave acceleration response was generally well predicted by both rotor inflow configurations; the most obvious anomaly occurring at the beginning of the input where the measured data exhibits an oscillatory behaviour not present in the simulation and possibly caused by an external disturbance.

b) Height rate response, the comparison of most immediate interest to flying qualities studies, was predicted well in trend but differed from the flight test data by a steady offset. This disparity may have been due to the fact that the aircraft is climbing slightly at the time of the collective input being applied.

c) A discrepancy in the prediction of yaw rate was attributed to the modelling of the gearing between the pilot's pedals and the tail rotor collective and the absence of sufficient aerodynamic damping. Other coupled responses were relatively poorly predicted. In addition, the simulated roll rate contained a low-frequency oscillation not apparent in the flight test which has been attributed to the coupling of rotor lead-lag motion with the roll axis.

With regard to the prediction of *rotor* aeromechanics :

a) Prediction of the rotor coning is fair in the short term and good in the longer term and in general correlates well with the normal acceleration comparisons.

b) Coning for the three state inflow model is greater than that for the six state model and this has been attributed to a higher concentration of thrust at the blade tips.

c) Further comparisons of rotor data throughout the manoeuvre indicate that the six state model offers superior predictions of both incidence and inflow distribution, although an increased number of spanwise modes is certainly required for simulation of the inflow near to the blade tip.

Overall, it is concluded that the Lynx test data and supporting analysis system has provided a valuable resource for current and future rotorcraft research studies at DERA.

ACKNOWLEDGEMENTS

The work described in this study was funded by the UK's Ministry of Defence within the Corporate Research Programme's Technology Group 3 entitled "Aerodynamics, propulsion, guidance and control".

The authors wish to express their thanks to Prof Alan Simpson for his invaluable advice and considerable effort in the application of SPA to the Lynx rotor.

REFERENCES

1) GOANKAR, G H; PETERS, David. *Review of dynamic inflow modelling for rotorcraft flight dynamics.* In: *Vertica* Vol. 12 No 3, 1988

2) TARTTELIN, Peter. *The DERA Bedford Lynx helicopter Research Instrumented Blades (LYNXRIBs).* (Unpublished DERA report), 1998.

3) HASSAL, Chris J.W. *Development and initial application of a technique to measure vibration mode shapes of a rotating blade.* (Unpublished DERA report), May 1977.

4) BROTHERHOOD, Philip. *The determination of helicopter blade normal force coefficient, incidence and stall boundaries from flight measurements of leading edge and trailing edge pressure.* (Unpublished DERA report), May 1993.

5) SUGRUE, Christian. *The Research Instrumented Blade Analysis (RIBAN) software package.* (Unpublished DERA report), 1998.

6) RILEY, John; PADFIELD Dr Gareth; SMITH, Jane. *Estimation of rotor blade incidence and blade deformation from the measurement of pressures and strains in flight.* Paper 110, 14th European Rotorcraft Forum, Milan, Italy, September 1988.

7) BURROWS, Andrew. *Lynx Strain-Gauged Blade ground vibration test at DRA Bedford,*

(DRA Contract No. FRN1c/580). Dynamics Research Group University of Manchester and British Aerospace Airbus Ltd. Report No. DRG-DRA-1-2/94, February 1994.

8) MILNE, Prof. Ronald; SIMPSON Prof. Alan. Theoretical and numerical assessment of strain pattern analysis. *Journal of sound and vibration*, 1996 192(1), 349-387.

9) SUGRUE, Christian. *Aerodynamic look-up tables for Lynx rotor blade analysis.* (Unpublished DERA report), June 1993.

10) TARTTELIN, Peter. *Flight trials in support of hi-fidelity simulation modelling using DERA Lynx ZD559 fitted with research instrumented blades - RAF Akrotiri.* (Unpublished DERA report), 1998.

11) *FLIGHTLAB Theory Manual*, Advanced Rotorcraft Technology Inc., 1997

12) PITT, Dale; PETERS, David. *Theoretical prediction of dynamic inflow derivatives. In: Vertica* Vol. 5 No 1, 1981

13) PETERS, David; BOYD, David; HE, ChengJiang. *Finite-state induced-flow model for rotors in hover and forward flight.* In: Journal of the American Helicopter Society Vol. 34 No 4, October 1989

14) HOUSTON, Stewart; TARTTELIN, Peter. *Validation of mathematical simulations of helicopter vertical response characteristics in hover. In: Journal of the American Helicopter Society* Vol. 36 No. 1, January 1991.

15) *Handling requirements for military rotorcraft. Aeronautical Design Standard 33D.* United States Army Aviation and Troop Command, Directorate for engineering, July 1994

16) TURNER, Graham. *A validation of the Helisim 3 flight mechanics model configured as a Lynx, for application to flying qualities prediction in hover.* (Unpublished DERA report), 1997.

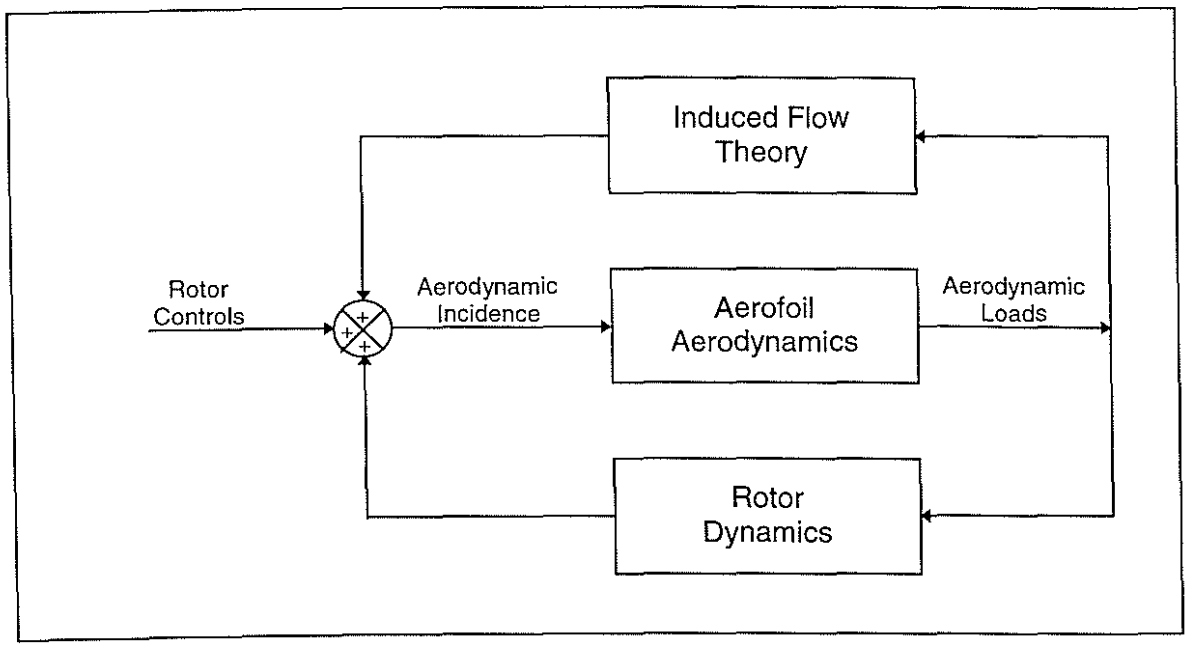

Figure 1; Schematic representation of rotor aeromechanics modelling

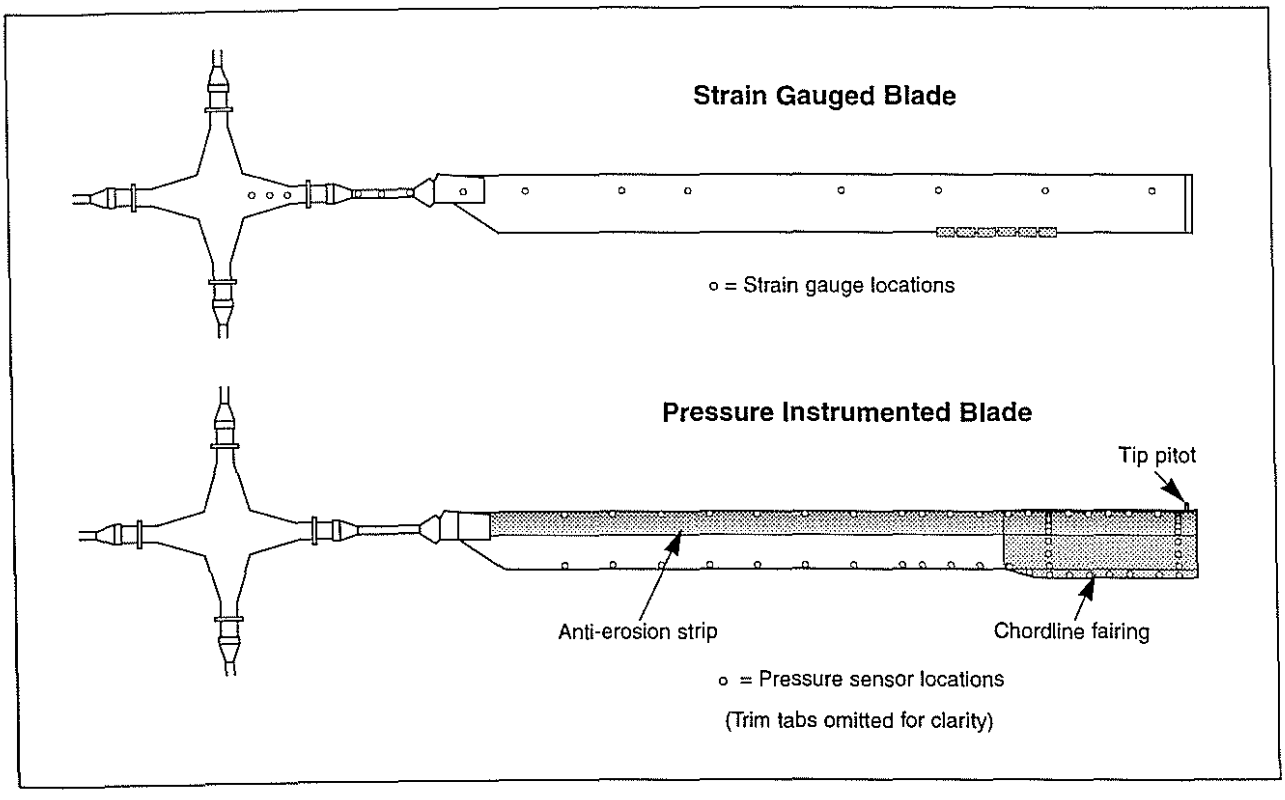

Figure 2; LYNXRIBs sensor locations

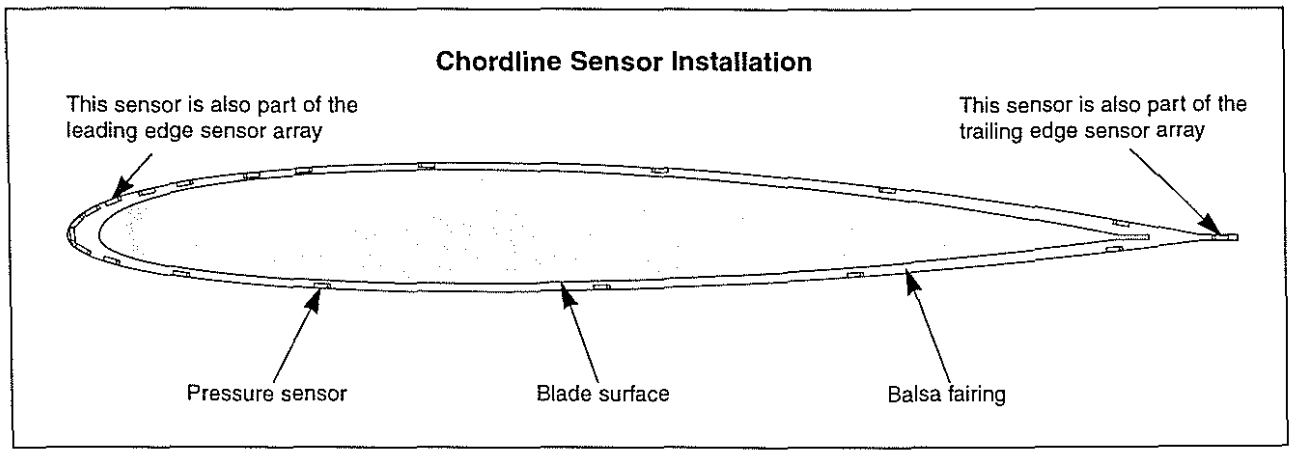

Figure 3; PIB chordline sensors at 85% radius

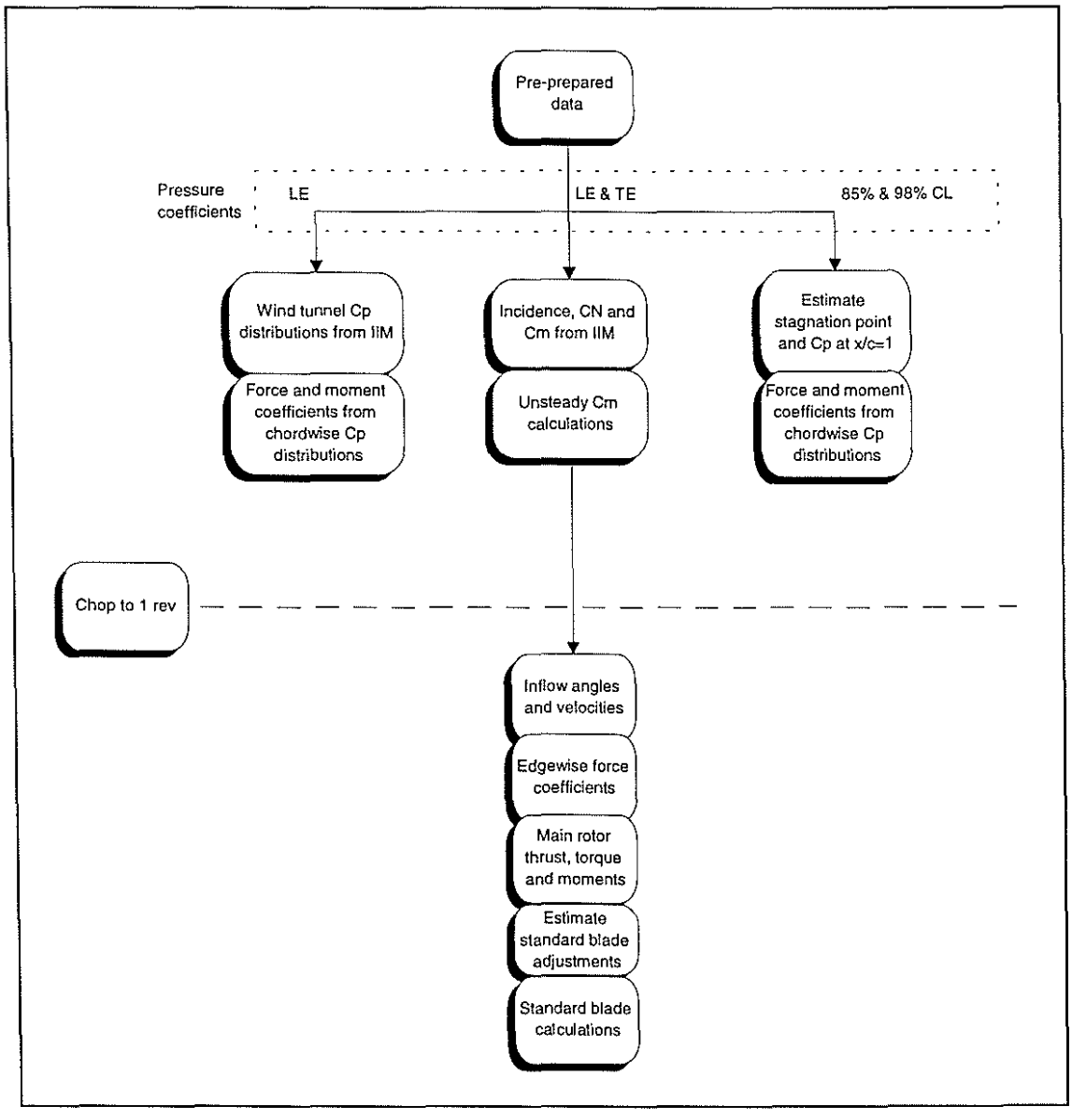

Figure 4; Flow of data through RIBAN during aerodynamics reconstruction

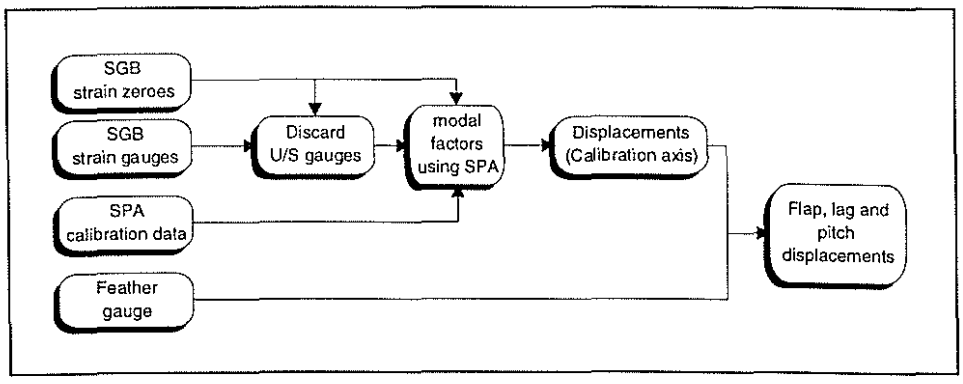

Figure 5; Flow of data through RIBAN during structural dynamics reconstruction

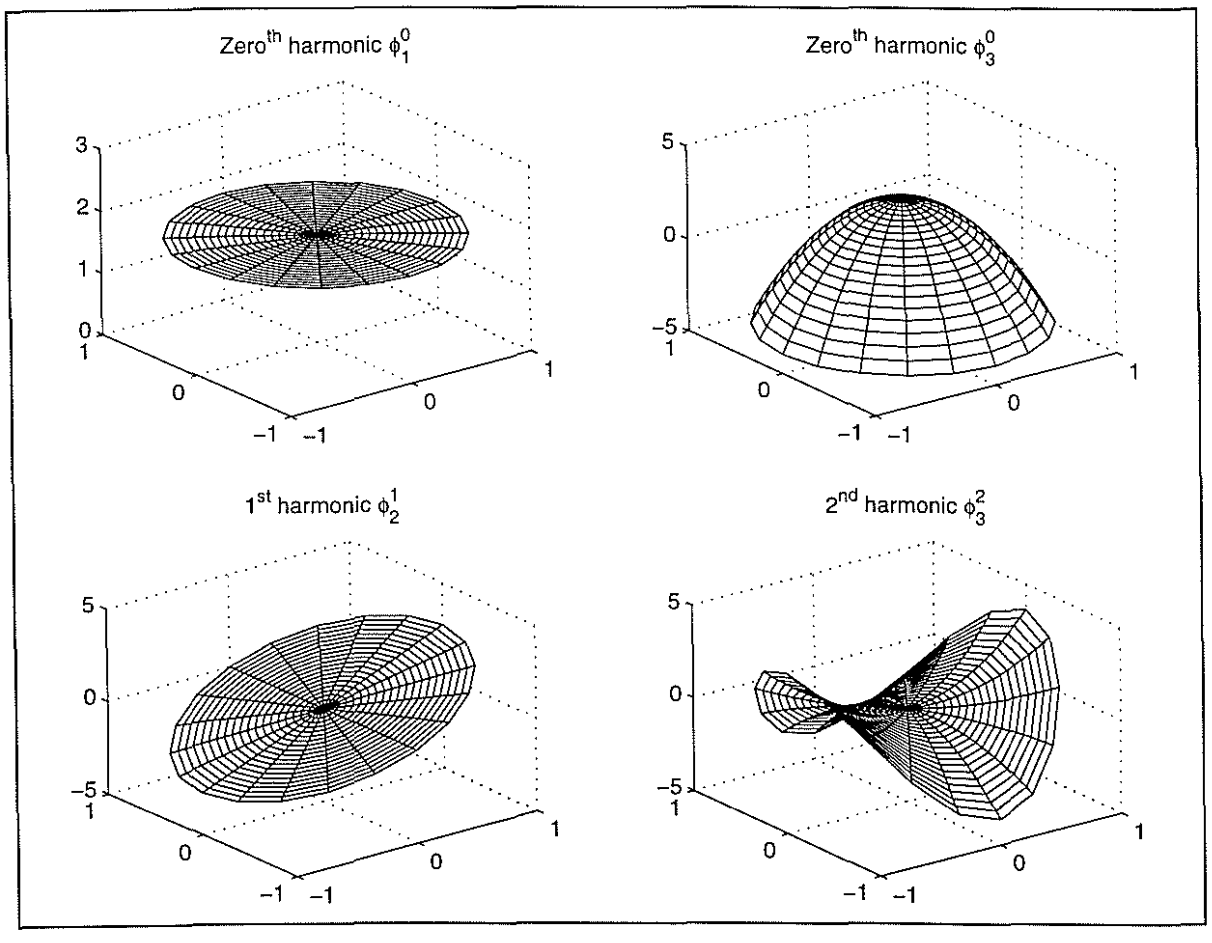

Figure 6; Representation of six state modes in three dimensions

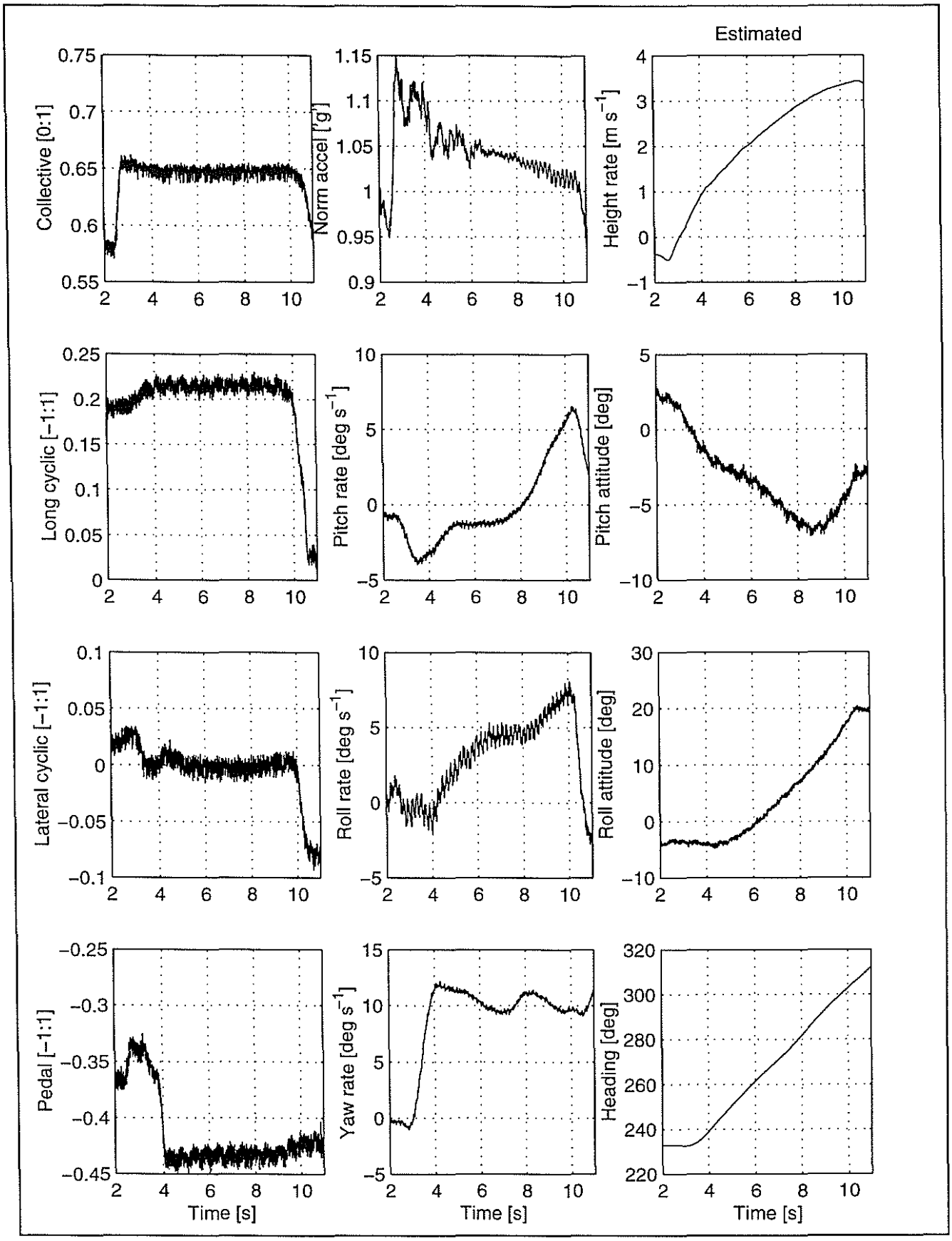

Figure 7; Aircraft response to collective step input

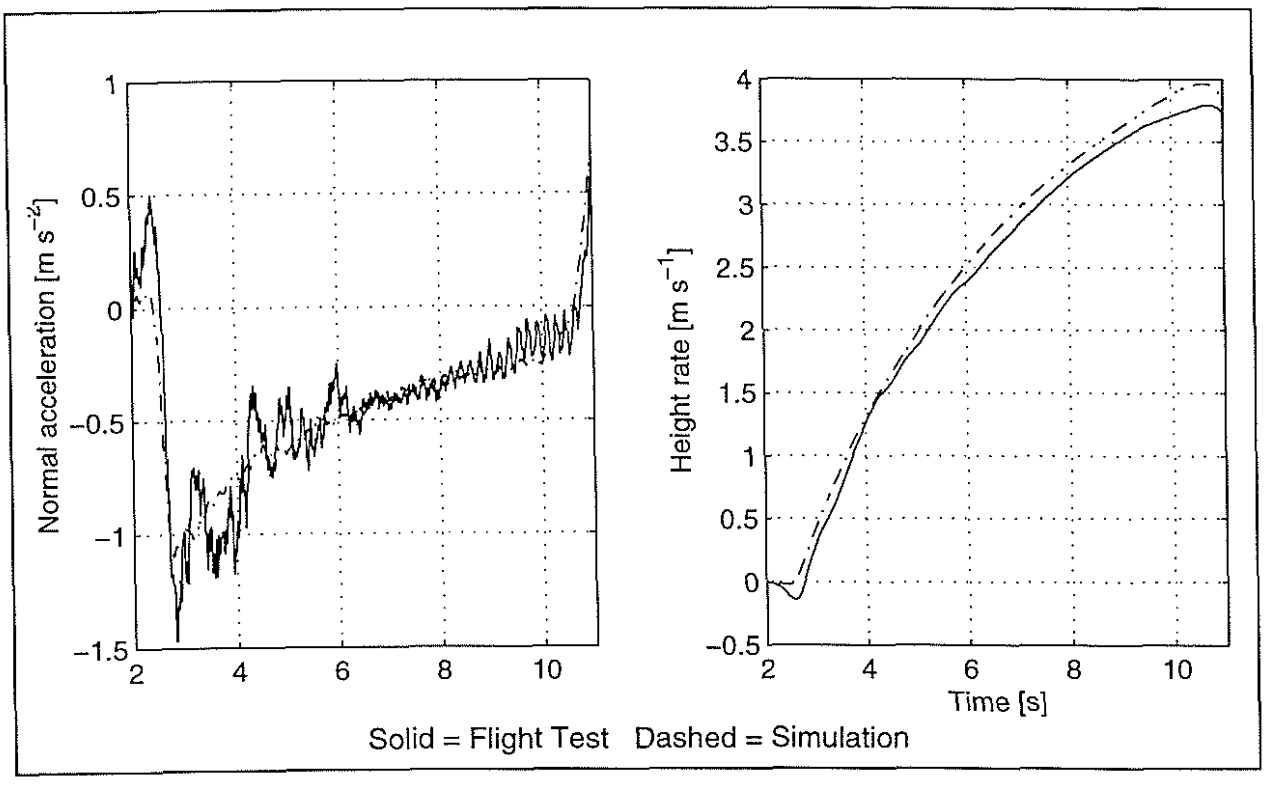

Figure 8; Comparison of identified heave responses with flight test

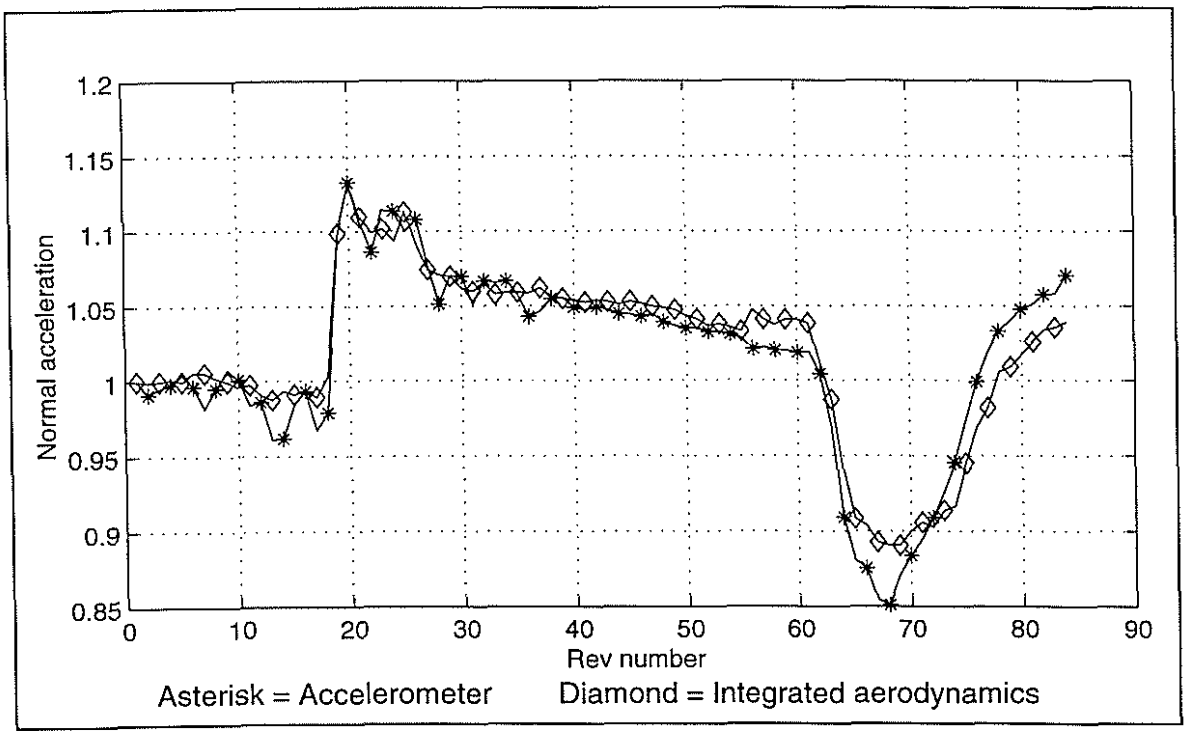

Figure 9; Comparison of calculated and measured normal acceleration

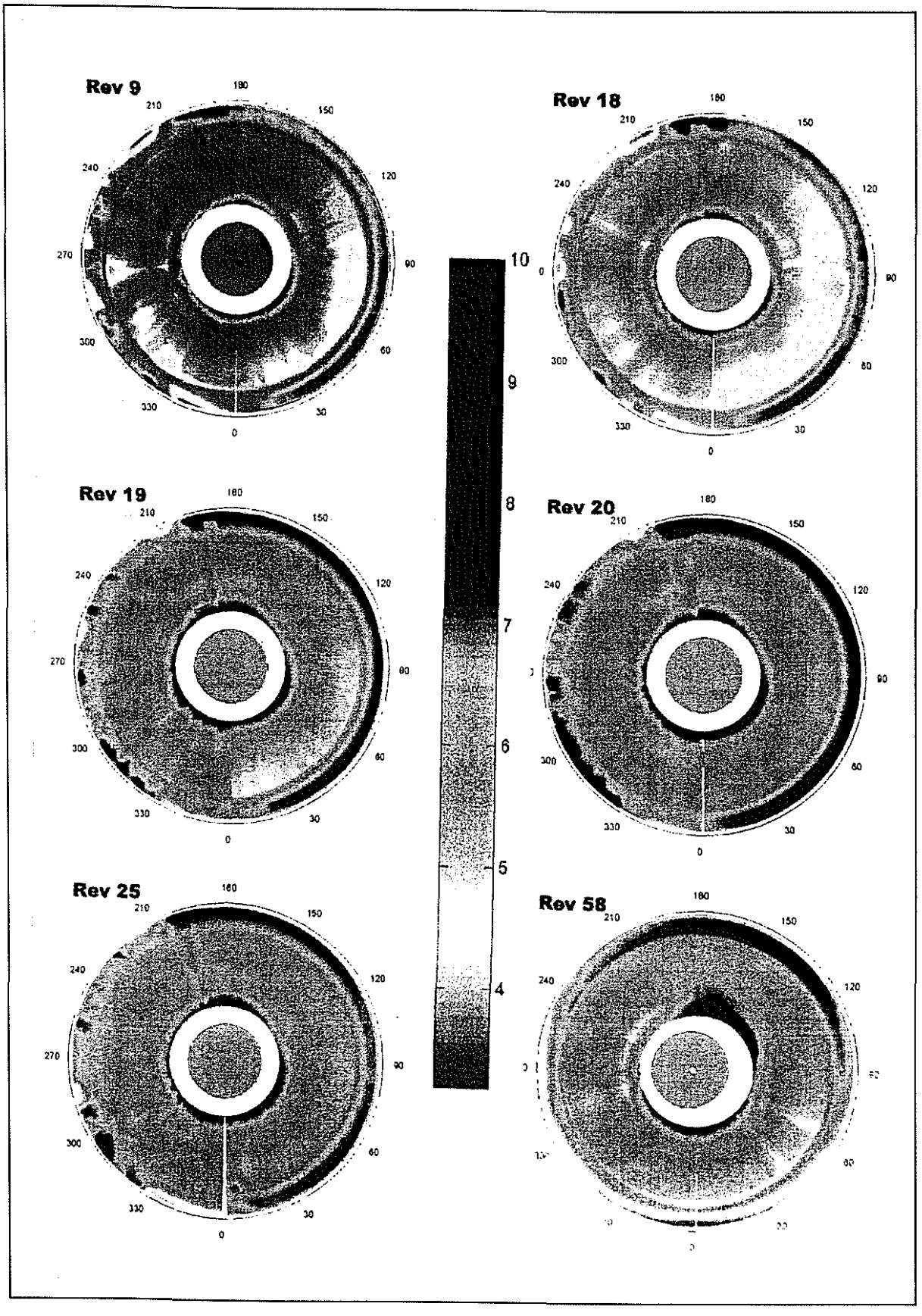

Figure 10; Polar plots of main rotor incidence

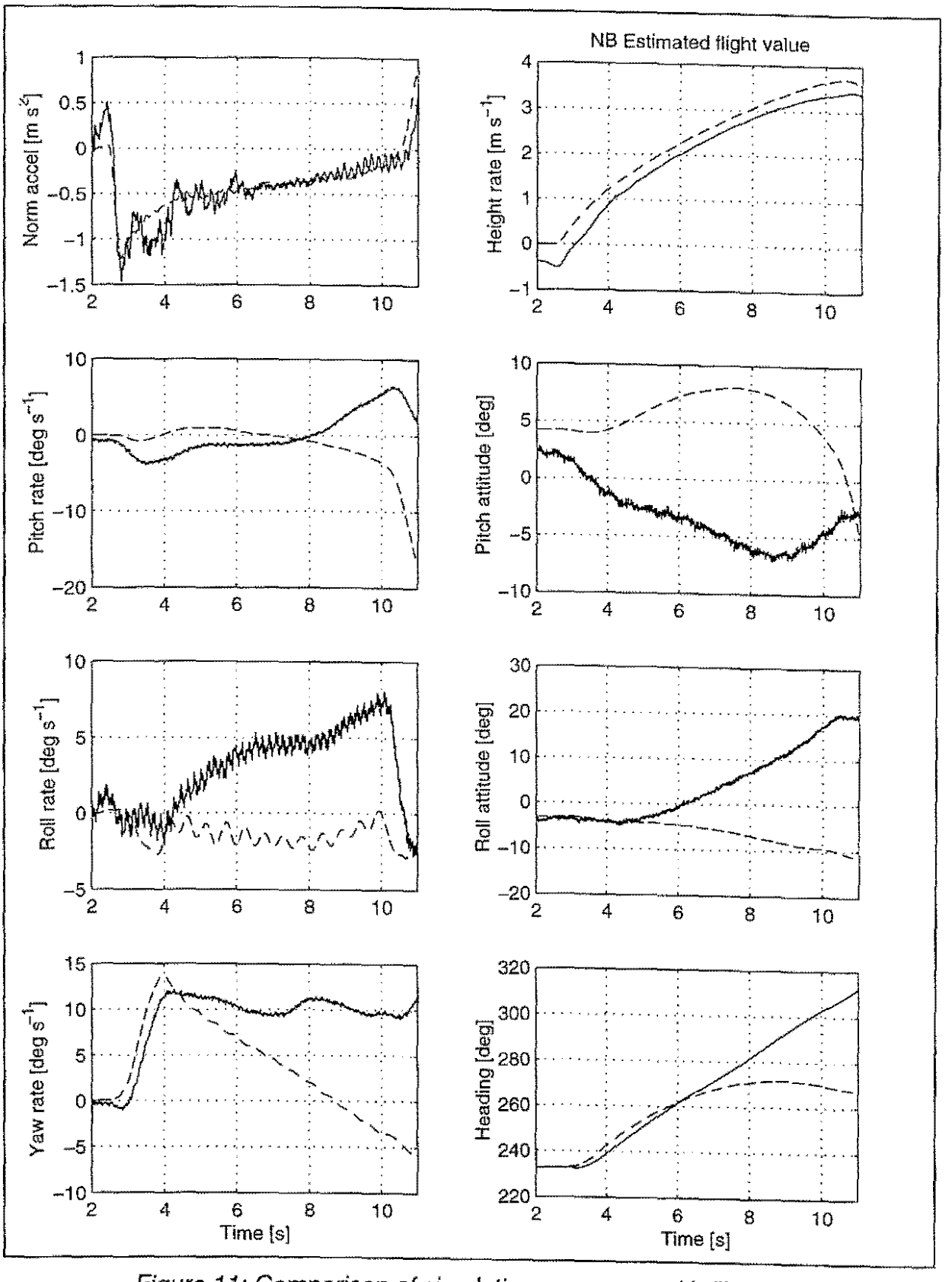

Figure 11; Comparison of simulation responses with flight test

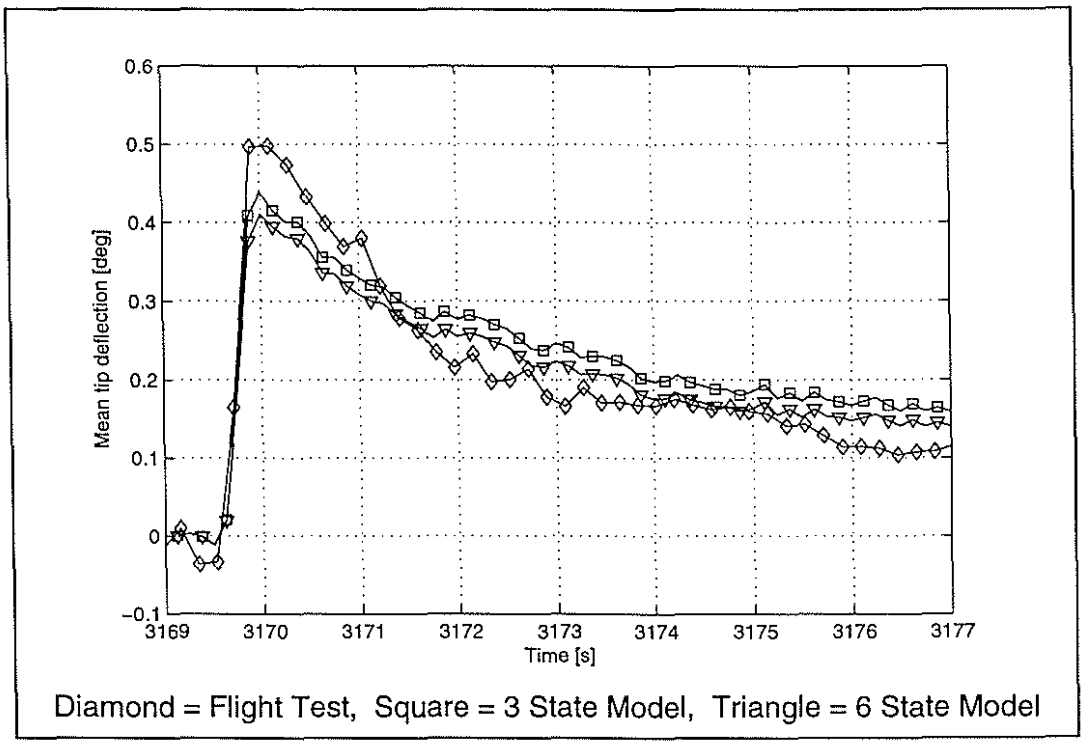

Figure 12; Comparison of simulated coning responses with flight test

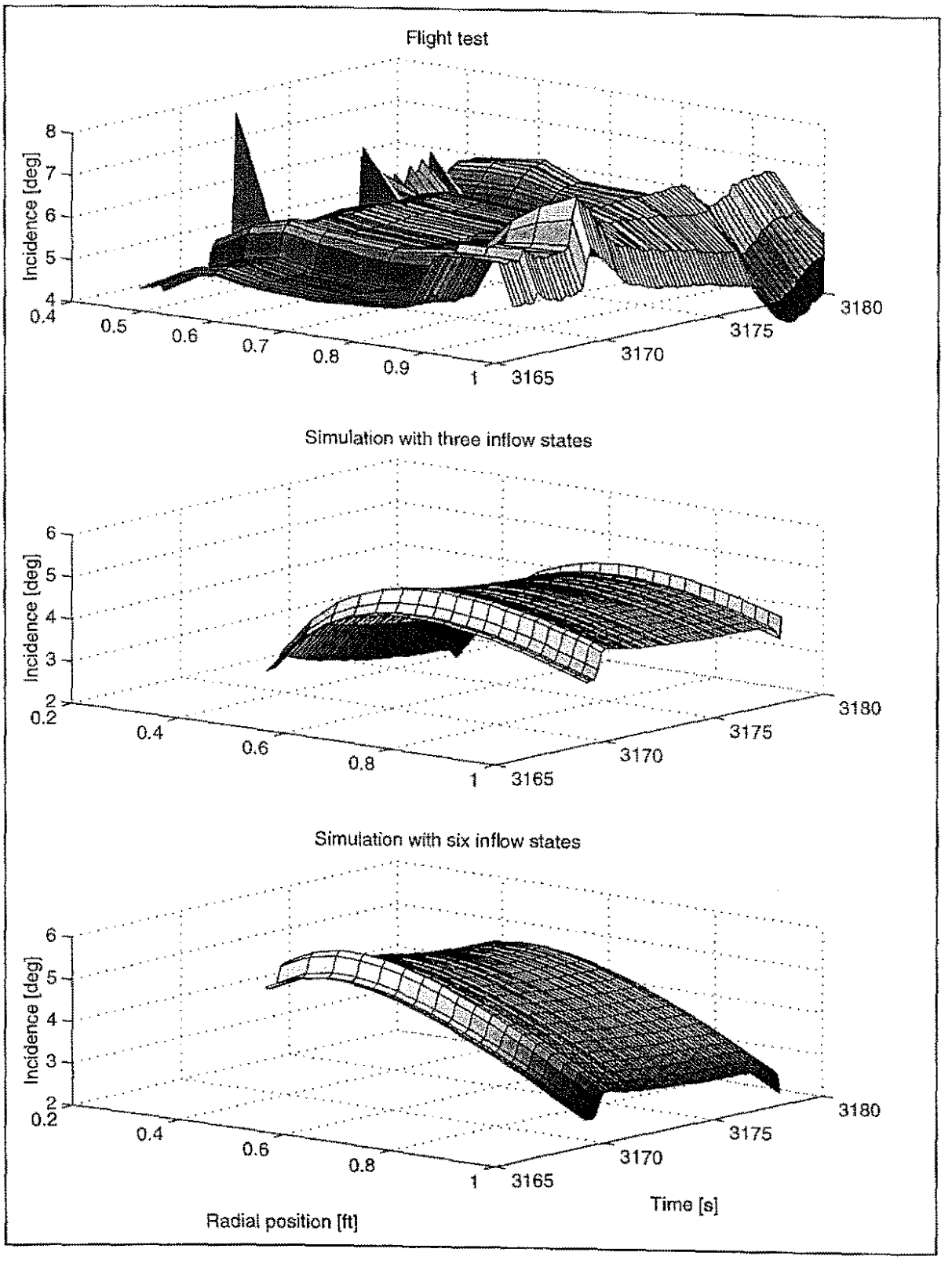

Figure 13; Three dimensional representation of incidence variation - F368 E19

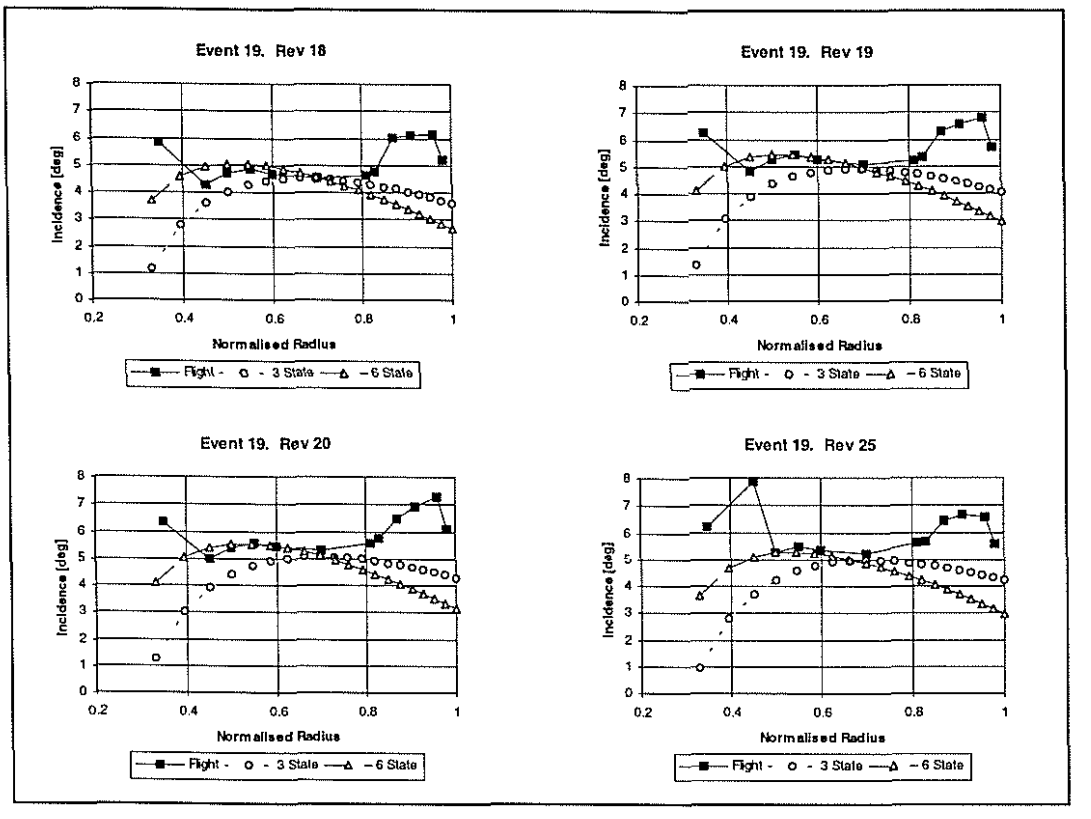

Figure 14; Comparison of averaged radial incidence distribution for selected rotor revs

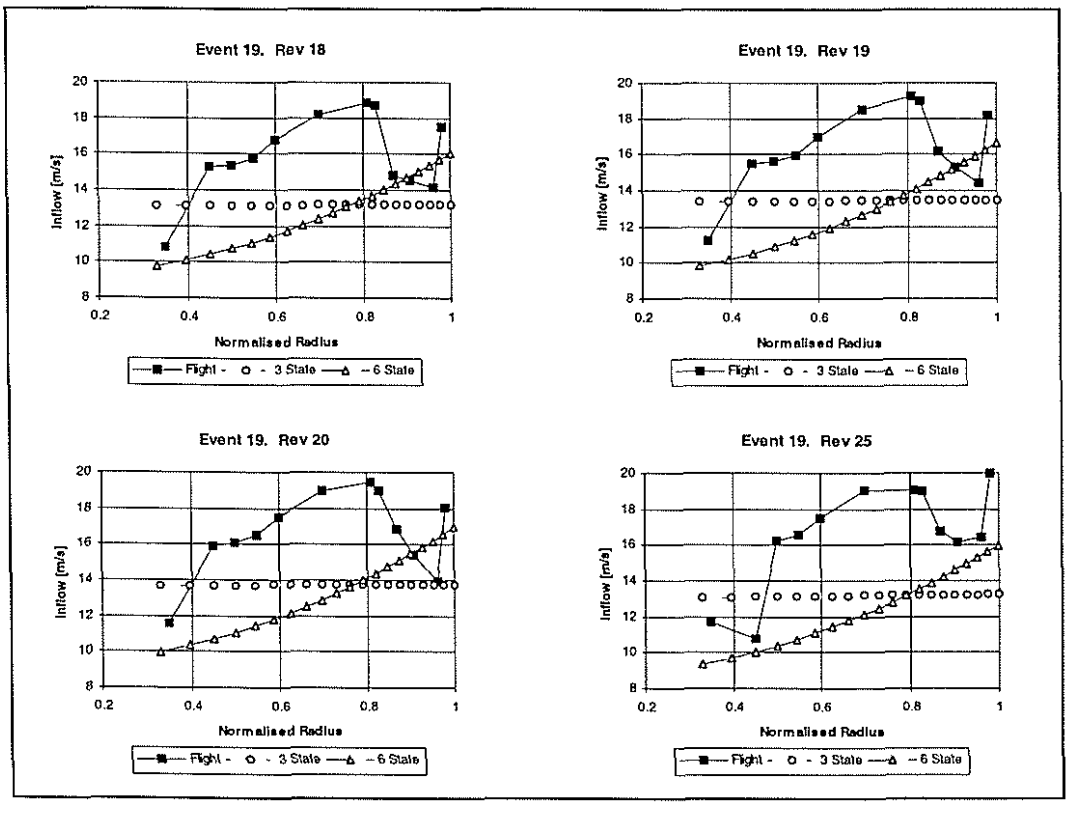

Figure 15; Comparison of averaged radial inflow distribution for selected rotor revs